International Journal for Multidisciplinary Research (IJFMR)
E-ISSN: 2582-2160 ● Website: www.ijfmr.com ● Email: editor@ijfmr.com

Influence of Praseodymium Doping On Structural, Microstructural and Elastic Properties of Nickel Ferrite Nanoparticles

Kajal A. Gurav[1], Sudarshan Gawali[2], Rahul Pandit[3], A.P. Keche[4], K. M. Jadhav[5]

[1,2]Department of Physics, Deogiri College, Chhatrapati Sambhajinagar – 431 005, (M.S.) India
[3,5]Physics Department, School of Basic and Applied Sciences, MGM University, Chhatrapati Sambhajinagar- 431 003, (M.S.) India
[4]Department of Physics, R. B. Attal Arts, Science and Commerce College, Georai, Beed - 431 127, (M.S.) India

Abstract:
In this communication, we present the influence of Praseodymium (Pr) doping on structural and elastic properties of nickel ferrite nanoparticles investigated through X-ray diffraction and Fourier transform infrared studies. The samples of $NiFe_{2-x}Pr_xO_4$ (x = 0.0, 0.025, 0.050, 0.075, 0.1) nanoparticles were prepared using a green synthesis approach in which Aegle marmelos was used as oxidizing and reducing agent. Single-phase formation with a cubic spinel structure was established through XRD analysis. The hopping length, bond length, interionic distances and bond angles increase with Pr doping, confirming the incorporation of Pr and its influence on structural properties. FTIR spectra also characterize the spinel structure formation by showing two prominent absorption bands. The elastic stiffness constant, Young's modulus. Bulk modulus and rigidity modulus determined from FTIR analysis show increasing trends with Pr doping. The longitudinal, transverse velocity, shear velocity and mean velocity show a decreasing trend with Pr doping in nickel ferrite. Thus, Pr doping in nickel ferrite influences the structural and elastic properties of nickel ferrite nanoparticles.

Keywords: Nickel ferrite, Pr doping, Structural properties, Elastic properties.

Introduction:

Ferrites are the most attractive magnetic material belonging to the ferrimagnetic group of oxides [1-3]. It is composed of metal oxides and iron oxides in a specific ratio. It crystallizes in three groups viz spinel ferrite, rare earth garnet and hexagonal ferrite [4]. In spinel ferrites, divalent metal ions and oxides like Cobalt, nickel, zinc, etc. are present [5]. In rare earth garnets, yttrium or rare earth ion oxides such as yttrium oxides, gadolinium oxides or dysprosium oxides, etc. are present [6]. In hexagonal ferrite, large metal ions such as barium, strontium, or calcium are present in oxide form [7]. Among the three groups of ferrites, spinel ferrites are a highly attractive candidate for several researchers. Spinel ferrite has the formula AB_2O_4, in which 'A' represents divalent metal ions, and 'B' represents the iron ion [8]. The crystal structure of spinel ferrite is similar to that of minerals spinel and has two interstitial sites commonly known

as tetrahedral (A) and octahedral [B] sites [9]. Spinel ferrites possess both electrical as well as magnetic properties, which can be tailored as per the desired application [10]. These properties of spinel ferrites are dependent on their synthesis procedure, synthesis conditions, and synthesis parameters. By controlling these parameters, the electrical and magnetic properties of spinel ferrites can be modified for new applications. The excellent electrical and magnetic properties of spinel ferrites lead to their utility in various applications, starting from the core of the transformer to the latest drug delivery application [11, 12].

In recent decades, research has been focused on the synthesis of spinel ferrite nanoparticles and their applications in gas sensors [13], hydrogen production [14], photocatalysis, magnetic hyperthermia [15], agriculture, environment, etc. The magnetic nanoparticles of spinel ferrite possess distinct properties such as nanosized dimensions, large surface area to volume, greater stability, biocompatibility, etc [16]. The properties of spinel ferrite nanoparticles are different compared to their bulk ferrite. At nanoscale, the material exhibits enhanced electrical, optical, magnetic, mechanical, etc. properties [17].

Nickel ferrite of the spinel ferrite family is most attractive and widely studied by many researchers for its potential applications in many fields. According to the literature survey, nickel ferrite possesses an inverse spinel structure, Ni ions occupying octahedral sites while Fe^{3+} ions are equally distributed among the tetrahedral A and B sites [18]. Nickel ferrite has the highest electrical resistivity as well as high saturation magnetization of the order of 81emu/gm and 10^5 to 10^8 Ω.cm respectively. Both electrical and magnetic properties depend on the distribution of cations over the tetrahedral A sites and B sites. The cation distribution in spinel ferrite is sensitive to the method of preparation, preparative parameters and conditions, crystallite size and nature of doping elements.

Wet chemical methods such as the sol-gel auto-combustion method are commonly used for the synthesis of spinel ferrite nanoparticles. This method requires organic fuels like citric acid, glycine, etc. auto combustion process [19]. Nitrates of metal are used as a raw material for the synthesis. During the combustion process, hazardous gases are liberated. Secondly, the nitrates are also costly. Considering these drawbacks of the sol-gel auto-combustion method, the green synthesis approach has gained a lot of attraction. The source of green fuel is usually plant extracts, algae, bacteria, etc., which are found easily and abundantly. The green fuel does not produce any harmful gases, and hence the green synthesis approach for the preparation of spinel ferrite nanoparticles has been increased.

Roberto Nistico et al. reported the hydrothermal synthesis of Cu-doped $NiFe_2O_4$ nanoparticles, where the spinel ferrite phase was preserved up to 50% Cu incorporation. Increased Cu content reduced the magnetic saturation and induced a redistribution of Fe ions between the tetrahedral and octahedral sites, as confirmed through Mössbauer analysis [20]. **Subiya Kazi et al.** reported the successful preparation of $NiFe_2O_4$ nanoparticles using the co-precipitation technique [21]. **A. Ahmed et al.** synthesized Pr^{3+}-substituted $Ni_{0.5}Co_{0.5}Fe_2O_4$ nanoparticles prepared by the sol–gel route, which exhibited a cubic spinel phase with crystallite sizes ranging from 9 to 17 nm. The incorporation of Pr^{3+} significantly altered their dielectric and magnetic properties, indicating their suitability for high-frequency energy-storage applications [22]. **Chaitali Mondal et al.** revealed the influence of thermal treatment on Pr^{3+}-modified nickel ferrite and found a strong correlation between sintering temperature and its structural, optical, and electrical characteristics. Higher sintering temperatures promoted crystallite and grain growth, altered dielectric behaviour, and reduced activation energy, highlighting the crucial role of thermal processing in tailoring the functional properties of Pr-doped nickel ferrites [23]. **Seyed Mahdi Peymani-Motlagh et al.** reports on Pr^{3+}- and Yb^{3+}-substituted cobalt–nickel ferrite nanoparticles synthesized by the sol–gel

auto-combustion method exhibited a spinel ferrite structure with minor rare-earth orthoferrite secondary phases. Rare-earth substitution significantly influenced the magnetic and photocatalytic performance, with Pr^{3+} improving magnetic properties, whereas Yb^{3+} enhanced the photocatalytic degradation efficiency of organic dyes [24]. **Dhafer O.Alshahrani et al.** report on Ni–Zn spinel ferrite nanoparticles synthesized through a green sol–gel route using pomegranate extract, demonstrating promising electrochemical performance for sustainable energy-storage applications [3]. **T. V. Sheena et al.** synthesized Ni–Co mixed spinel ferrite nanoparticles using Vitex negundo leaf extract and demonstrated their potential for targeted drug delivery and bio-separation applications [25]. **Yasir Amrilloh et al.** synthesized $NiFe_2O_4$ nanoparticles through a green hydrothermal route using Uncaria gambir Roxb. leaf extract, which exhibited reduced particle size and enhanced magnetic characteristics. The green-synthesized ferrite achieved up to 98% phosphate removal, demonstrating its potential as an efficient and sustainable material for environmental remediation [26].

The literature survey revealed that nickel ferrite has been prepared in nanosized dimensions using different wet chemical methods like chemical co-precipitation and hydrothermal methods, investigated for structural, morphological, surface optical and magnetic properties. However, the detailed investigations of structural and elastic properties of nickel ferrite prepared by Aegle marmelos leaves have not been reported in the literature. Furthermore, the effect of rare earth and Pr^{3+} ions on the structural and elastic properties of nickel ferrite are not systematically reported in the literature, which is essential to correlate the electrical, optical, and magnetic properties. Here, we report the structural and elastic properties of Pr doped nickel ferrite nanoparticles synthesized via Aegle marmelos leaves extract-assisted sol-gel auto-combustion method.

2. Experimental

2.1 Materials

Praseodymium Pr^{3+}-doped nickel ferrite nanoparticles with the chemical formula $NiFe_{2-x}Pr_xO_4$ (x = 0.000, 0.025, 0.050, 0.075, and 0.100) were synthesized using high-purity analytical-grade precursors. Ferric nitrate nonahydrate ($Fe(NO_3)_3 \cdot 9H_2O$, 99.1%), nickel nitrate hexahydrate ($Ni(NO_3)_2 \cdot 6H_2O$,99.0%), and praseodymium (III) nitrate hexahydrate ($Pr(NO_3)_3 \cdot 6H_2O$, 99.9%) were procured from HPLC India Pvt. Ltd. and used without any further purification. Aegle marmelos (Bel) leaf extract was employed as a biogenic fuel and reducing agent in the green sol–gel auto-combustion synthesis process.

2.2 Preparation of Aegle marmelos Extract

Fresh Aegle marmelos leaves were cleaned thoroughly, naturally dried under sunlight, and pulverized into a fine powder. A measured quantity of the powdered leaves was added to distilled water and continuously stirred at 80 °C to extract the phytochemical constituents. After heating, the solution was allowed to cool to approximately 300 K and filtered using Whatman No. 42 filter paper. The obtained clear filtrate was subsequently used as a biogenic extract for nanoparticle synthesis

2.3 Green Synthesis of $NiFe_{2-x}Pr_xO_4$ (x = 0.0, 0.025, 0.050, 0.075, 0.1) NPs

Praseodymium-doped nickel ferrite nanoparticles, $NiFe_{2-x}Pr_xO_4$ (x = 0.0, 0.025, 0.050, 0.075, 0.1), were synthesized by a green sol–gel auto-combustion method. Stoichiometric amounts of nickel nitrate hexahydrate, ferric nitrate nonahydrate, and praseodymium nitrate nonahydrate were dissolved in 200 mL of distilled water under continuous magnetic stirring. Aegle marmelos leaf extract was added as a natural fuel, and the pH was adjusted to 7 using dilute ammonia. The resulting solution was heated at 80 °C with constant stirring until a homogeneous gel was obtained. The gel was then heated to 120 °C, at which point

it self-combusted, yielding a fine precursor powder. Finally, the powder was calcined at 800 °C for 8 h to enhance crystallinity, remove residual organic species, and obtain phase-pure spinel $NiFe_{2-x}Pr_xO_4$ nanoparticles.

3. Characterizations

The structural and vibrational properties of the synthesized Pr^{3+}-doped $NiFe_2O_4$ nanoparticles were investigated using a range of characterization techniques. Phase purity and crystal structure were examined by X-ray diffraction (XRD) at room temperature (300 K) using a Rigaku Miniflex 600 diffractometer equipped with Cu-Kα radiation (λ = 1.5406 Å). The diffraction patterns were recorded over a 2θ range of 10°–90°. Fourier transform infrared (FTIR) spectroscopy was carried out using a Bruker Alpha II spectrometer to identify the characteristic vibrational modes of the samples. The spectra were collected in the wavenumber range of 400–4000 cm^{-1} at ambient temperature (300 K).

4. Results and Discussion

X-Ray diffraction (XRD)

The samples of Pr^{3+} doped nickel ferrite with generic formulae $NiFe_{2-x}Pr_xO_4$ (x = 0.0, 0.025, 0.050, 0.075, 0.1) were structurally characterized by the X-ray diffraction method (XRD). The XRD patterns were recorded within the 2θ range of 20º to 80º at room temperature. The 3D crystal structure of Pr-doped nickel ferrite is shown in **Fig. 1**. The analysis of the XRD pattern revealed the single-phase formation with a cubic spinel structure. The details of the XRD analysis were reported in our previous communication.

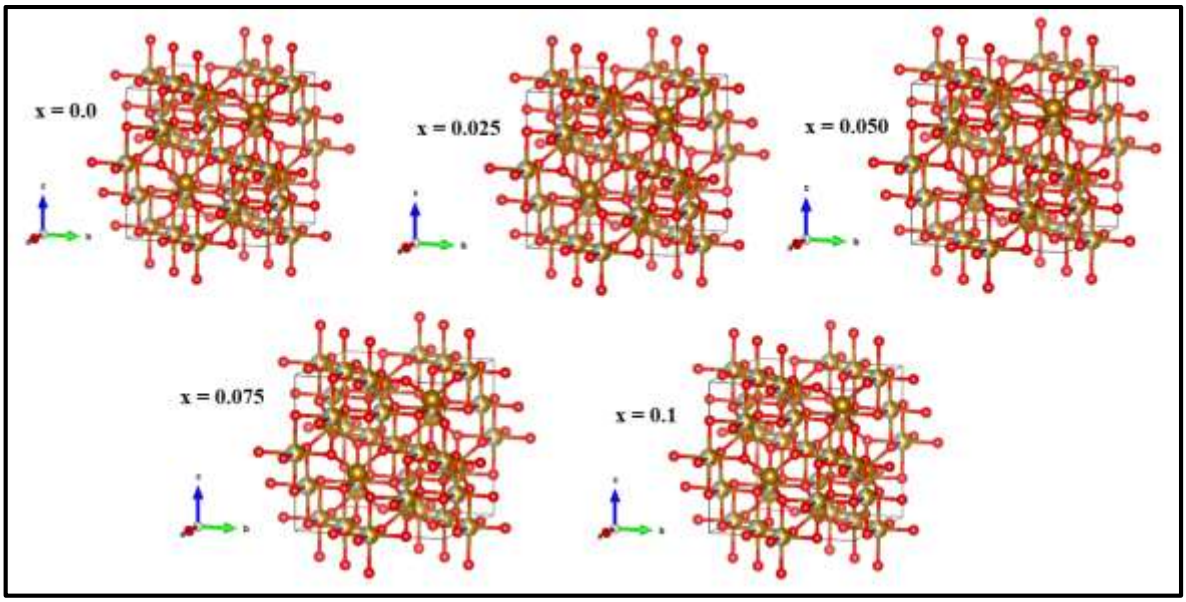

Fig 1. 3D crystal structure of $NiFe_{2-x}Pr_xO_4$ (x = 0.0, 0.025, 0.050, 0.075, 0.1) nanoparticles unit cell projected along the standard orientation of crystal shape.

The values of hopping lengths (L_A and L_B) were calculated using the following formulas [27] and the values are presented in **Table 1.** The variation of hopping length with Pr doping is shown in Fig. 2
Hopping length:

$$L_A = a\sqrt{\frac{3}{4}}\text{Å} \quad (1)$$

$$L_B = a\sqrt{\frac{2}{4}}\text{Å} \quad (2)$$

The ionic radii of the tetrahedral and octahedral interstitial lattice sites (r_A and r_B) were calculated using the following relations [28] and are listed in **Table 1**

Ionic radii:

$$r_A = \left(u - \frac{1}{4}\right) a\sqrt{3} - r(O^{2-})\text{Å} \quad (3)$$

$$r_B = \left(\frac{5}{8} - u\right) a - r(O^{2-})\text{Å} \quad (4)$$

From **Table 1,** the parameters L_A, L_B and r_A and r_B exhibit a slight increase with increasing Pr^{3+} concentration, suggesting a marginal expansion of the spinel crystal lattice. This trend is attributed to the larger ionic radius of Pr^{3+} relative to Fe^{3+}, which results in increased cation–oxygen bond lengths and ionic radii. The negligible changes in these structural parameters indicate that the cubic spinel framework is preserved, confirming the successful incorporation of Pr^{3+} ions into the $NiFe_2O_4$ lattice without causing significant structural distortion.

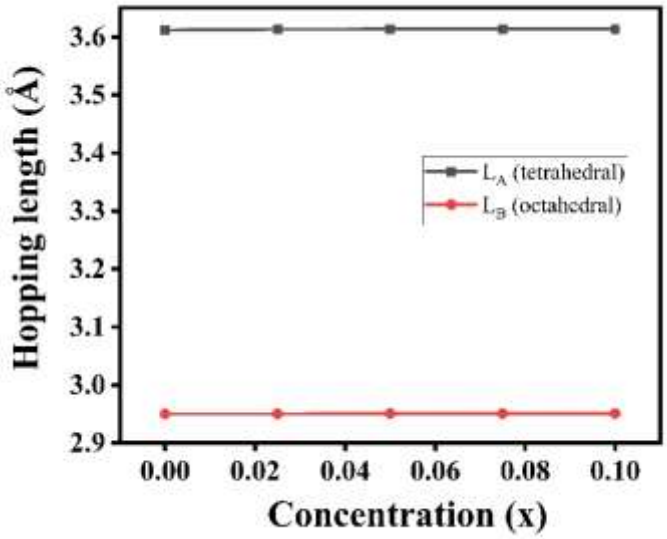

Fig 2. Variation of hopping lengths with Pr concentration

Table 1. Values of hopping length for A-site (L_A), hopping length of B-site (L_B), tetrahedral ionic radii (r_A), and octahedral ionic radii (r_B) of $NiFe_{2-x}Pr_xO_4$ (x = 0.0, 0.025, 0.050, 0.075, 0.1) spinel ferrite NPs

x	L_A (Å)	L_B (Å)	r_A (Å)	r_B (Å)
0.000	3.612	2.950	0.573	0.716
0.025	3.613	2.950	0.573	0.716
0.050	3.614	2.951	0.574	0.716
0.075	3.614	2.951	0.574	0.717
0.100	3.614	2.951	0.574	0.717

The bond lengths associated with the tetrahedral and octahedral interstitial lattice sites (d_{AX} and d_{BX}) were determined using the following formulas [29] and are listed in **Table 2**

Tetrahedral bond length: $d_{AX} = a\sqrt{3\left(u - \frac{1}{4}\right)}$ Å (5)

Octahedral bond length: $d_{BX} = a\sqrt{3u^2 - \frac{11}{4}u + \frac{43}{64}}$ Å (6)

The tetrahedral edge-shared (d_{AXE}) and octahedral edge-shared/unshared (d_{BXE} and d_{BEU}) bond lengths were calculated using the following relations [30] and are summarized in **Table 2**

Tetraedge shared: $d_{AXE} = a\sqrt{2\left(2u - \frac{1}{2}\right)}$ Å (7)

Octaedge shared: $d_{BXE} = a\sqrt{2(1-2u)}$Å (8)

Octaedge unshared: $d_{BEU} = a\sqrt{4u^{2-}3u + \frac{11}{16}}$ Å (9)

The values of tetrahedral and octahedral bond lengths, tetrahedral and octahedral edge sharing distance and octahedral unsharing distance show a gradual increase with increasing Pr^{3+} content. This trend is attributed to the larger ionic radius of Pr^{3+} relative to Fe^{3+}, which results in a slight expansion of the spinel lattice. The variations in these structural parameters indicate that the cubic spinel framework remains stable, confirming the successful incorporation of Pr^{3+} ions into the $NiFe_2O_4$ lattice without causing noticeable structural distortion.

Table 2. Values of tetrahedral bond length (dAX), octahedral bond length (dBX), tetraedge shared (dAXE), Octaedge shared (dBXE), Octaedge unshared (dBEU) of $NiFe_{2-x}Pr_xO_4$ (x = 0.0,0.025,0.050,0.075,0.1) spinel ferrite NPs

x	d_{AX} (Å)	d_{BX} (Å)	d_{AXE} (Å)	d_{BXE} (Å)	d_{BEU}(Å)
0.000	1.893	2.037	3.091	2.808	2.951
0.025	1.893	2.037	3.092	2.809	2.952
0.050	1.894	2.038	3.092	2.809	2.952
0.075	1.894	2.038	3.093	2.810	2.953
0.100	1.894	2.038	3.093	2.809	2.953

The distances between intrinsic ions, namely [cations (metal ions) – anions (oxygen ions)] (p, q, r, s) and [cations (metal ions) – cations (metal ions)] (b, c, d, e, f), were determined using the following formulas and are presented in **Tables 3 and 4**

Interionic distance: $p = a\left(\frac{5}{8} - u\right)$ Å (10)

$q = a\sqrt{3}\left(u - \frac{1}{4}\right)$ Å (11)

$r = a\sqrt{3}\left(u - \frac{1}{4}\right)$ Å (12)

$s = a\sqrt{3}\left(\frac{u}{3} + \frac{1}{8}\right)$ Å (13)

$b=\sqrt{2}\left(\frac{a}{4}\right)$Å (14)

$c=\sqrt{11}\left(\frac{a}{8}\right)$ Å (15)

$d=\sqrt{3}\left(\frac{a}{4}\right)$ Å (16)

$e=\sqrt{3}\left(\frac{3a}{8}\right)$ Å (17)

$f=\sqrt{6}\left(\frac{a}{4}\right)$ Å (18)

Table 3. Values of Interionic distances (p, q, r, s) of $NiFe_{2-x}Pr_xO_4$ (x = 0.0, 0.025, 0.050, 0.075, 0.1) spinel ferrite NPs

x	p (Å)	q (Å)	r Å)	s (Å)
0.000	2.036	1.893	3.625	3.641
0.025	2.036	1.893	3.626	3.642
0.050	2.036	1.894	3.626	3.643
0.075	2.037	1.894	3.627	3.643
0.100	2.037	1.894	3.626	3.643

Table 4. Values of Interionic distances (b, c, d, e, f) of $NiFe_{2-x}Pr_xO_4$ (x = 0.0, 0.025, 0.050, 0.075, 0.1) spinel ferrite NPs

x	b(Å)	c(Å)	d(Å)	e(Å)	f(Å)
0.000	2.950	3.459	3.612	5.419	5.109
0.025	2.950	3.460	3.613	5.420	5.110
0.050	2.951	3.450	3.614	5.421	5.111
0.075	2.951	3.461	3.614	5.422	5.112
0.100	2.951	3.460	3.614	5.421	5.111

From **Tables 3 and 4,** it can be observed that the intrinsic distance values gradually increase with the increasing substitution of Pr^{3+} ions.

The Interionic angle value is calculated by the following formulae, and the values are given in Table 5.

$\theta_1 = \cos -1 \left(\frac{p^2+q^2-c^2}{2pq}\right)$ (19)

$\theta_2 = \cos -1 \left(\frac{p^2+r^2-e^2}{2pr}\right)$ (20)

$$\theta_3 = \cos -1 \left(\frac{2p^2+b^2}{2p^2}\right) \quad (21)$$

$$\theta_4 = \cos -1 \left(\frac{p^2+s^2-f^2}{2ps}\right) \quad (22)$$

$$\theta_5 = \cos -1 \left(\frac{r^2+q^2-d^2}{2rq}\right) \quad (23)$$

Table 5. Values of Bond angles (Θ_1, Θ_2, Θ_3, Θ_4 and Θ_5) of Ni $Fe_{2-x}Pr_xO_4$ (x = 0.0, 0.025, 0.050, 0.075, 0.1) spinel ferrite NPs

x	Θ_1	Θ_2	Θ_3	Θ_4	Θ_5
0.000	123.290	146.902	123.303	125.867	74.451
0.025	123.290	146.902	123.303	125.867	74.451
0.050	123.290	146.902	123.303	125.867	74.451
0.075	123.290	146.902	123.303	125.867	74.451
0.100	123.290	146.902	123.303	125.867	74.451

Fourier transform infrared spectroscopy (FTIR)

Pr doped nickel ferrite nanoparticles were characterized by the Fourier transform infrared spectroscopy technique. The analysis of FTIR spectra revealed the characteristic features of spinel ferrite reported in our previous communication.

The Debye temperature of all the Pr^{3+} doped nickel ferrite nanoparticles was calculated by using the following relation, where the value of λc for the ferrite materials was taken as 1.438.

$\Theta_1 = \lambda c \upsilon_{av} = 1.438 \upsilon_{av}$ (24)

The term υ_{av} represents the average wavenumber of the bands. The Debye temperature values are listed in **Table 6**, which indicates that doping nickel ferrite nanoparticles with Pr^{3+} ions leads to an increase in the Debye temperature.

3.3 Elastic properties

Typically, materials have 36 elastic moduli, but for isotropic and homogeneous materials like spinel ferrites and garnets, this can be simplified to three independent elastic constants [31]. The stiffness constant C_{11} was computed using the following relation:

Stiffness constant: $C_{11} = \frac{k}{a}$ (25)

Where k is the average force constant, and a is the lattice constant. The stiffness constant is derived using Poisson's ratio in combination with the elastic stiffness constant.

Stiffness constant $C_{12} = \frac{\sigma \times C_{11}}{(1-\sigma)}$ (26)

Where C_{11} and C_{12} are stiffness constants, and σ is the Poisson ratio. The values of both C_{11} and C_{12} are listed in **Table 6.**

Elastic moduli for the cubic structure were evaluated using the relation:

Young's modulus was determined using the following relation

Young's modulus (E)= $\frac{(C_{11}-C_{12})(C_{11}+2C_{12})}{(C_{11}+C_{12})}$ (27)

Here, the stiffness constant is denoted as (C_{12}), and the elastic stiffness is represented as (C_{11}). The bulk modulus is expressed as follows:

Bulk modulus (K)= $\frac{1}{3}(C_{11}+2C_{12})$ (28)

Rigidity modulus (G)= $\frac{E}{2(\sigma+1)}$ (29)

Where E is Young's modulus. It can be observed from **Table 6** that the value of Young's modulus, Bulk modulus, and Rigidity modulus increases with an increase in Pr^{3+} in nickel ferrite nanoparticles.

Table 6. Debye temperature (θ_D) Values of elastic stiffness constant (C_{11}), stiffness constant (C_{12}), Young's modulus (E), bulk modulus (K), Rigidity modulus (G) for the FTIR spectrum of $NiFe_{2-x}Pr_xO_4$ (x = 0.0, 0.020.050, 0.075, 0.1) spinel ferrite NPs

x	θ_D (K)	C_{11} (GPa)	C_{12} (GPa)	E (GPa)	K (GPa)	G (GPa)
0.000	662.92	128.22	69.04	79.89	88.76	29.58
0.025	666.51	130.03	70.01	81.01	90.01	30.00
0.050	682.33	137.63	74.10	85.75	95.28	31.76
0.075	687.36	140.88	75.86	87.78	97.53	32.51
0.100	690.24	143.17	77.09	89.20	99.11	33.03

The longitudinal velocity (V_L) and shear wave velocity were calculated using the following equation values shown in **Table 7.**

Longitudinal velocity (V_L)= $\left(\frac{C_{11}}{\rho}\right)$ (30)

Shear velocity (V_s)= $\left(\frac{G}{\rho}\right)^{1/2}$ (31)

Transversal elastic wave velocity (V_t) = $\sqrt{\frac{C_{11}}{3\rho}}$ (32)

Where (V_t) represents the velocity of the transverse elastic wave, and ρ represents the X-ray density. (C_{11}) represents the elastic stiffness.

The mean elastic wave velocity is calculated with the help of the (V_t) transversal elastic wave velocity and (V_L) longitudinal velocity by the following formula, and values are given in **Table 7.**

Mean velocity = $\left[\frac{1}{2}\left(\frac{2}{V_t^3}+\frac{2}{V_l^3}\right)\right]^{\frac{-1}{3}}$

Table 7. Values of longitudinal velocity (V_l), Transversal velocity (V_t), and shear velocity (V_s), mean wave velocity (V_m), and the FTIR spectrum of $NiFe_{2-x}Pr_xO_4$ (x = 0.0, 0.025, 0.050, 0.075, 0.1) spinel ferrite NPs

x	V_l (m/s)	V_t (m/s)	V_s (m/s)	V_m (m/s)
0.000	4890.5	2823.4	2349.4	3134.5
0.025	4905.2	2831.5	2356.3	3143.6
0.050	5021.5	2900.8	2412.2	3220.3
0.075	5058.4	2922.5	2429.9	3244.4
0.100	5079.4	2932.8	2440.1	3256.0

Conclusion:

The green synthesis approach has been effectively utilized to prepare the Pr doped nickel ferrite nanoparticles. The single-phase nature was confirmed through XRD analysis. The structural parameters such as hopping length, tetrahedral radius, octahedral radius, etc show a strong influence of Pr doping. The elastic parameters such as stiffness constant, Young's modulus, etc shoe dependence on Pr doping. The green synthesis approach also influences the structural and elastic properties of Pr-doped nickel ferrite.

Acknowledgments

The author, Kajal Gurav, acknowledges the Mahatma Jyotiba Phule Research & Training Institute (MAHAJYOTI-2022) for the fellowship support. The author also expresses gratitude to the Department of Chemistry, Dr Babasaheb Ambedkar Marathwada University, Chhatrapati Sambhajinagar, for providing FTIR measurements.

References

1. AlGharram, M., et al., *Dimensionality-Controlled Structure and Magnetism in Nickel Ferrite (NiFe2O4): A Novelty-Oriented Theoretical Review.* Magnetochemistry, 2026. **12**(6): p. 69.
2. Anantharamaiah, P., et al., *Critical rare-earth Yb3+ solubility, magnetic tuning and enhanced low-field magnetostriction in sintered CoFe2-xYbxO4 ceramics.* Journal of Magnetism and Magnetic Materials, 2026: p. 174428.
3. Alshahrani, D.O., M. Arslan, and M. Saad, *Green sol-gel synthesis of Ni-Zn spinel ferrites using pomegranate extract for enhanced energy storage application.* Ceramics International, 2026.
4. Pathare, R.N., et al., *Rare-Earth Doping in CdFe2O4 Spinel Ferrites: A Comprehensive Study of Structural, Elastic, Vibrational and Magnetic Properties.* Micro and Nanostructures, 2026: p. 208802.
5. Swetha, P. and R. Sagayaraj, *A Comprehensive Review on the Synthesis, Characterization, and Applications of Spinel Ferrite Nanoparticles.* A Comprehensive Review on the Synthesis,

Characterization, and Applications of Spinel Ferrite Nanoparticles, 2026: p. 74-102.
6. Neupane, D., et al., *Rare-Earth Doped Gd3− x RE x Fe5O12 (RE= Y, Nd, Sm, and Dy) Garnet: Structural, Magnetic, Magnetocaloric, and DFT Study.* Ceramics, 2023. **6**(4): p. 1937-1976.
7. Godara, S.K., et al., *Sol-gel auto-combustion method for the synthesis and investigation of Zr4+/Cu2+ doped barium calcium M-type hexaferrites.* Journal of Sol-Gel Science and Technology, 2025. **116**(3): p. 1821-1832.
8. Sushant, S., et al., *Development of M–NiFe2O4 (Co, Mg, Cu, Zn, and rare earth materials) and the recent major applications.* International Journal of Self-Propagating High-Temperature Synthesis, 2023. **32**(2): p. 61-116.
9. Sagar, A., et al., *Structural, optical, and photocatalytic properties of Ni–Zn and Mg-Zn spinel ferrites.* Interactions, 2024. **245**(1): p. 86.
10. Ahmad, U., et al., *Improved magnetic and electrical properties of transition metal doped nickel spinel ferrite nanoparticles for prospective applications.* Materials Science in Semiconductor Processing, 2022. **148**: p. 106830.
11. Abdel Maksoud, M.I.A., et al., *Insights on magnetic spinel ferrites for targeted drug delivery and hyperthermia applications.* Nanotechnology Reviews, 2022. **11**(1): p. 372-413.
12. Wani, S.M., et al., *Effect of titanium doping on structural, morphological, optical, magnetic and antibacterial properties of zinc ferrite.* Materials Science and Engineering: B, 2026. **324**: p. 118975.
13. Dey, B., et al., *Exploring the effect of zinc substitution in nanocrystalline nickel ferrite for enhanced supercapacitor and gas sensing applications.* Ceramics International, 2024. **50**(7): p. 12121-12135.
14. Tiwari, S., et al., *Spinel Ferrite-Based Materials for Electrochemical Applications: Synthesis, Applications, and Future Perspectives.* arXiv preprint arXiv:2607.10823, 2026.
15. Krishnan, Y., et al., *Spinel cobalt ferrite nanoparticles for photocatalysts, sensor and biomedical applications: a review.* Semiconductors, 2024. **58**(9): p. 721-739.
16. Ojha, V.H., et al., *Classification of Ferrites, Synthesis and Properties of Spinel Ferrite Nanoparticles and Their Applications*, in *Handbook of Materials Science, Volume 2: Magnetic Materials*. 2024, Springer. p. 103-146.
17. Shobana, M., et al., *Influence of Gd doping on the structural, optical, dielectric, and magnetic properties of ZnFe2O4: a combined experimental and theoretical study.* Ceramics International, 2025. **51**(5): p. 6748-6761.
18. Naveed-Ul-Haq, M. and S. Hussain, *Pressure-induced structural, electronic, and magnetic evolution in cubic inverse spinel NiFe2O4, an ab-initio study.* Applied Physics A, 2022. **128**(1): p. 30.
19. Longchar, C., A.R. Xavier, and D. Nath, *Synthesis of ferrite nanomaterials: a comparative analysis of sol-gel auto-combustion and co-precipitation methods-a review.* Research Digest on Engineering Management and Social Innovations (p-ISSN: 3117-4418 e-ISSN: 3117-4426), 2025. **1**(2): p. 29-48.
20. Nistico, R., et al., *Hydrothermal synthesis of Cu-substituted Ni ferrites: Structural, morphological, and magnetic properties.* Journal of Alloys and Compounds, 2024. **981**: p. 173628.
21. Kazi, S., et al., *Simple Co-precipitation synthesis and characterization of magnetic spinel NiFe2O4 nanoparticles.* Materials Today: Proceedings, 2023. **73**: p. 448-454.
22. Ahmed, A., et al., *Praseodymium doped Ni-Co based spinel ferrite nanoparticles prepared for energy storage applications.* Physica B: Condensed Matter, 2025. **700**: p. 416947.

23. Mondal, C., A. Dutta, and A. Sinha, *Structural interpretation of sintering temperature effect on optical and electrical properties of Pr3+-Substituted nickel ferrites.* physica status solidi (a), 2023. **220**(17): p. 2300263.
24. Peymani-Motlagh, S.M., et al., *Assessing the magnetic, cytotoxic and photocatalytic influence of incorporating Yb3+ or Pr3+ ions in cobalt–nickel ferrite.* Journal of Materials Science: Materials in Electronics, 2019. **30**(7): p. 6902-6909.
25. Sheena, T., B. Jyothish, and J. Jacob, *Green synthesis and characterization of nanocrystalline Ni-Co spinel ferrites using Vitex negundo leaf extract for biomedical applications.* Next Materials, 2026. **11**: p. 101717.
26. Amrulloh, Y., et al., *Feasible synthesis of nickel ferrite using Uncaria gambir Roxb. leaf extract for removal of phosphate from aqueous solution.* Results in Surfaces and Interfaces, 2025. **18**: p. 100404.
27. Vani, K., et al., *Impact of rare earth Tb3+ substitution in cobalt ferrites: Tuning structural, dielectric, magnetic properties and photocatalytic activity.* Ceramics International, 2025. **51**(1): p. 240-251.
28. Gawali, S., et al., *Influence of Y3+ and Cr3+ co-doping on the structural, vibrational, elastic, morphology and magnetic properties of cobalt ferrite nanoparticles.* Journal of Superconductivity and Novel Magnetism, 2025. **38**(6): p. 243.
29. Wanjari, S.S., et al., *Investigating impact of Ni-Cd substitution on structural magnetic and optical properties of nanosize Al ferrites.* Heliyon, 2024. **10**(21).
30. Venu, S., et al., *Magnetic properties, structural investigation and optical studies of Er3+ doping Cd-Mg spinel ferrite.* Applied Physics A, 2024. **130**(8): p. 567.
31. Hasan, S. and B. Azhdar, *Synthesis and investigation of structural, elastic, and electrical properties of cobalt and magnesium substituted Ni–Zn spinel ferrite nanoparticles.* Journal of Physics: Condensed Matter, 2023. **35**(42): p. 425303.